SAND77-0582
Unlimited Release

OPTICAL Analysis of Solar Facility Heliostats

Eugene A. Igel, Robert L. Hughes

Prepared by Sandia Laboratories, Albuquerque, New Mexico 87115
and Livermore, California 94550 for the United States Energy Research
and Development Administration under Contract AT(29-1)-789

Printed May 1977

Sandia Laboratories

SF 2900 Q(7-73)

Issued by Sandia Laboratories, operated for the United States Energy Research & Development Administration by Sandia Corporation.

NOTICE

SF 1004-DF (3-75)

Printed in the United States of America
Available from
National Technical Information Service
U. S. Department of Commerce
5285 Port Royal Road
Springfield, VA 22161
Price: Printed Copy $4.00; Microfiche $3.00

SAND77-0582
(Unlimited Release)
Printed May 1977

Optical Analysis of Solar Facility Heliostats

E. A. Igel
R. L. Hughes
Optics Division 2541
Sandia Laboratories
Albuquerque, New Mexico 87115

Abstract

An experimentally verified simple analytical model, based on classical optical aberrations, is derived and predicts the power reception of a central receiver solar facility. A laboratory simulation was made of a typical heliostat, and its images were photographed and measured at several angles of incidence. The analytically predicted image size is in agreement with experiment to within less than 10% over an incident angle range of 60 degrees. Image size for several of the heliostats in the Sandia-ERDA Solar Thermal Test Facility array were calculated throughout a day and compared with ideal images and the size of the receiver. The optical parameters of the system and the motion of the sun were found to severely affect the design and optimization of any solar thermal facility. This analysis shows that it is the aberration astigmatism which governs the solar image size at the receiver. Image growth is minimal when heliostats are used at small angles of incidence, which usually corresponds to a limited operating time of two to three hours. However, image size is markedly increased at large angles of incidence which, unfortunately, occur when system operation is extended to a large fraction of a day over all seasons, as will be required for electric power producing facilities. There is no optically unique heliostat design, but sophistication of design must be tailored to heliostat location, size, and operational time interval as well as to receiver size. Obvious modifications to the optical surface which are intended to optimize performance are of only limited effectiveness and in fact can lead to images larger than those from a simple spherical surface at large angles of incidence. The principal result of this study is that the predominant sources of image enlargement are identified and measures for minimizing these enlargements are presented. This analysis considers only the idealized optical problem and does not consider the pragmatic errors associated with implementation and operation of a heliostat array.

Contents

Illustrations

Illustrations (Continued)

Optical Analysis of Solar Facility Heliostats

Introduction

The Sandia-ERDA Solar Thermal Test Facility (STTF) is currently under construction to document the important engineering parameters that dictate economic feasibility of a Solar Thermal Electric Facility. Historically the idea of generating electric power from solar thermal power is not new.[1] Current rationale for a solar tower electric facility has been documented by Sandia-ERDA[2,3] and while other similar proposals[4,5] have been made, the merit of generating electric power from a central-receiver thermal-cycle will not be discussed. Our interest in this aspect of solar energy is limited to describing basic optical considerations and, in particular, the dominant aberration, astigmatism, and how it relates to the overall problem of collecting and concentrating energy at a central receiver. Astigmatism associated with off-axis imaging is well known but not commonly understood. It is important to visualize this aberration as related to parameters of the Sandia-ERDA STTF. In this evaluation errors produced by facet figure and heliostat-facet shapes and tracking are only incidentally considered. Others[6] have considered this problem in some detail. It is fundamental geometric optics and the resultant image defects that are presented along with a simple analytical model to describe these defects. Severe limitations are established with few and expensive alternatives for meeting ideal goals.

Field & Model Heliostat Specifics

An intermediate test of the Sandia-ERDA facility is to be a four-megawatt thermal test using 222 heliostats. The layout of the heliostat-field and central tower-receiver is shown in Fig. 1. Each square heliostat frame which tracks the

sun to reflect insolation to the tower receiver is approximately 6 meters by 6 meters. There are twenty-five square facets, each approximately 1.2 meters by 1.2 meters, individually attached to the heliostat frame and which because of their preformed concave spherical shape optimally focus the sun's rays at the receiver.

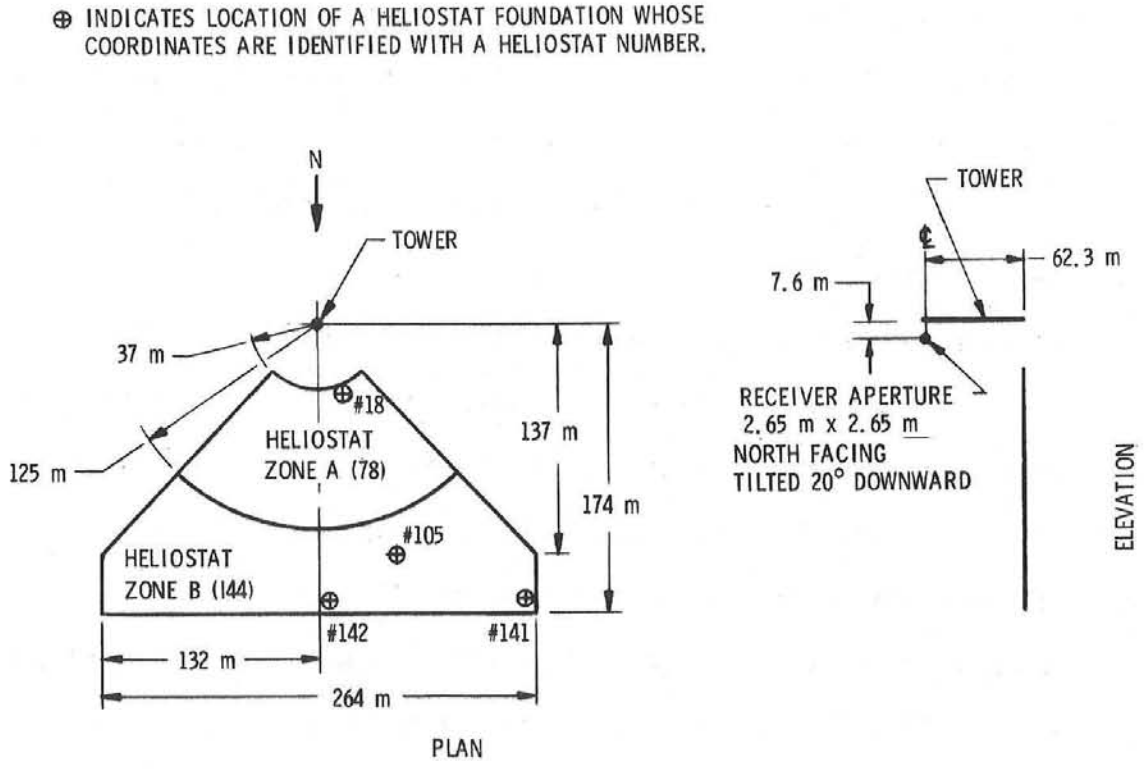

FIG. 1 STTF PLOT FOR MARTIN-MARIETTA RECEIVER, FOUR MEGAWATT THERMAL TEST.

Each heliostat tracks the sun to maintain the image location at the receiver. As the sun position changes throughout the day so does the angle of incidence, i.e., the angle between a ray from the sun and the normal to the heliostat's center facet. When a heliostat operates at angles of incidence greater than zero (the usual operating condition) the resultant image increases in size. This increase is attributed to the optical aberration of astigmatism and if the enlarged image is greater than the size of the tower-receiver then power reduction results. A laboratory mock-up

of a typical STTF-heliostat was made and is schematically shown in Fig. 2. An

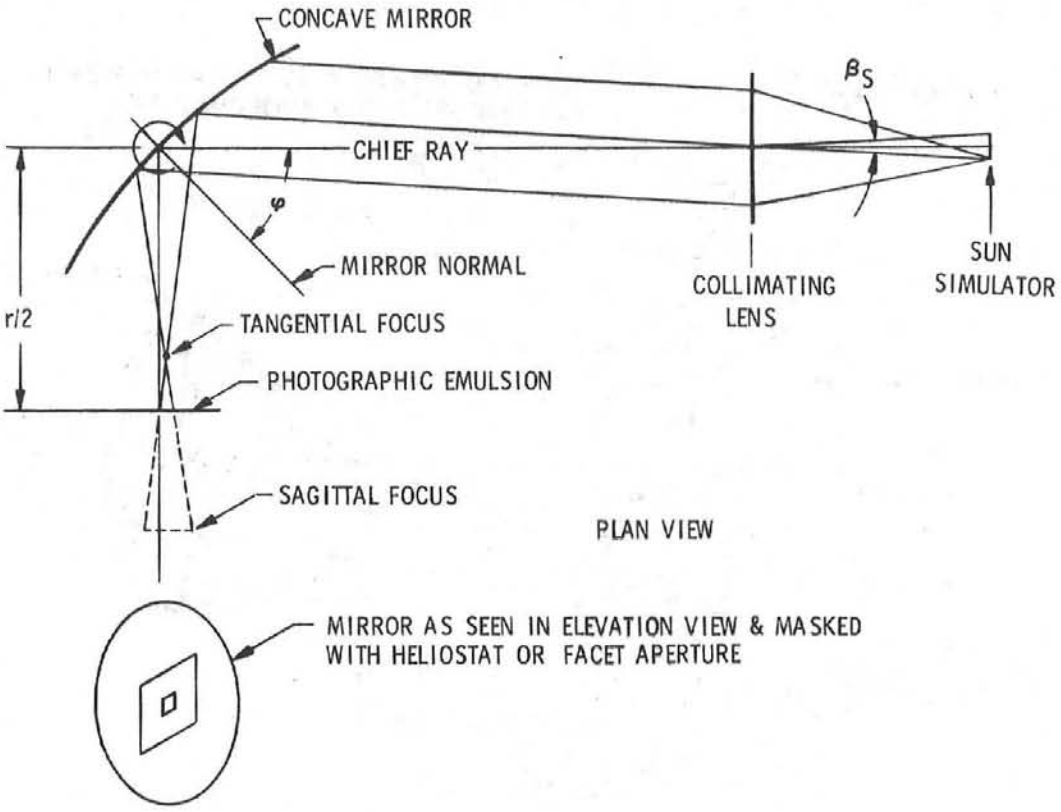

FIG. 2 LABORATORY MOCK-UP FOR TYPICAL STTF HELIOSTAT

incandescent source subtending the same angle as the sun viewed from earth, β_s = 9.3 milliradians, was used to irradiate a concave spherical mirror masked to optically simulate either a facet or a heliostat. This lab-heliostat gave a focal-ratio, F_r, (focal distance/heliostat height or width) of 16 and a facet focal-ratio of 80, corresponding to a STTF heliostat having an approximate slant range of 97 meters. The laboratory heliostat was rotated through a wide range of incident angles and photographs of the resultant images were taken at a slant range or focal distance of one-half the radius of curvature of the mirror, 400 millimeters. An off-axis bundle of rays is drawn to show the edge of the image at the tangential focus in the plan-view of Fig. 2. These rays diverge and in

the absence of the photographic emulsion contribute to the image at the sagittal focus. Fig. 3 indicates more clearly this astigmatic effect.

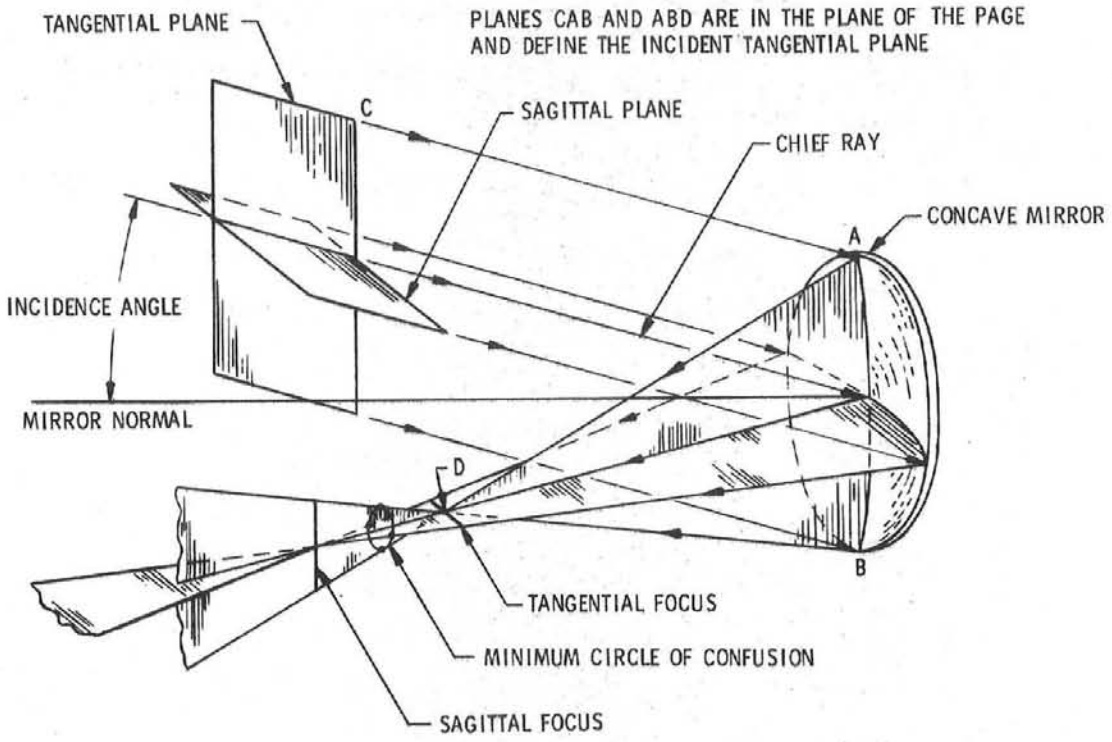

FIG. 3 DIAGRAM SHOWING THE ASTIGMATIC FOCI FOR A CONCAVE MIRROR AT OBLIQUE ANGLE OF INCIDENCE.

Astigmatic Optical Performance

Fig. 4 shows the photographed size of the astigmatic images from a laboratory facet and heliostat. The images at $\varphi = 0$ were not photographed but were visually measured at 3.7 millimeters and this value may be used as the scale to determine the linear increase of images at other values of φ. Note that STTF specification allows the perfect image of the sun to increase only a maximum of 33% from all error sources. Heliostat images at $\varphi = 30°$ show in addition to the irradiance envelope at the r/2 focal distance the envelopes at the tangential (T) and sagittal (S) foci which give a measure of relative image sizes. Notice that images

SQUARE FACET

SIDE = 5 MM

RADIUS = 800 MM

F_r = 80

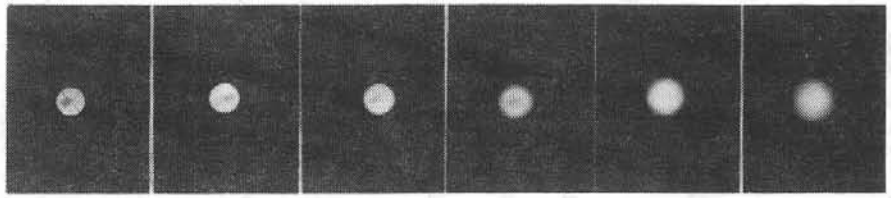

ANGLE OF INCIDENCE, φ 10° 20° 30° 40° 50° 60°

(T)

SQUARE HELIOSTAT

SIDE = 25 MM

RADIUS = 800 mm

F_r = 16

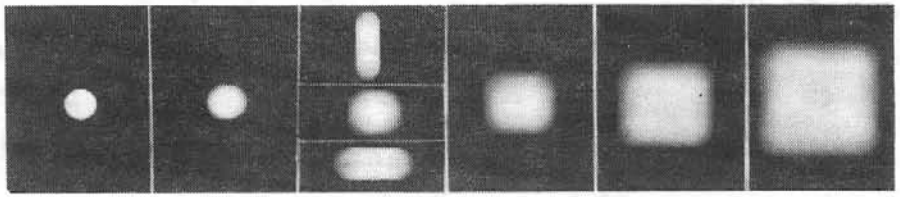

(S)

FIG. 4 SIMULATED SUN IMAGES FROM LABORATORY FACET AND HELIOSTAT CORRESPONDING TO A STTF FACET OR HELIOSTAT AT A 97 METER SLANT RANGE. THE IMAGE DIAMETER AT φ = 0° IS 3.7 MILLIMETERS.

corresponding to those produced by the single facet alone, $F_r = 80$, are the minimum sized images which would be obtained from a STTF-heliostat at a slant range of 97 meters if each of its facets were tracking the sun.

Modeling of the optical performance, whether a facet or heliostat, is accomplished by application of the Coddington equations[7,8] which describe the basic relationship of object-image conjugates as a function of angle of incidence. Equations and geometry are illustrated in Fig. 5. Fig. 5a is drawn with the tangential fan of incident and reflected rays in the plane of the page which is also the plane of incidence. The tangential focal line is normal to the page and the image width, w, is normal to the chief ray and lies in the tangential fan or incident plane. Conversely, the fan of rays of Fig. 5b are at right angles to those of Fig. 5a. Here the sagittal focal line is normal to the sagittal ray fan and the image height, h, is normal to the chief ray and lies in the sagittal fan. Note that r is the radius and D is the diameter of the concave mirror and that the image conjugates, S'_s and S'_t, are measured from the mirror-vertex and along the chief-ray (CR). From the geometry the following equations are derived when the object distance, S, equals infinity.

Sagittal Conjugate, S'_s,	=	$r(\sec \varphi)/2$
Tangential Conjugate, S'_t,	=	$r(\cos \varphi)/2$
Astigmatic Difference, $S'_s - S'_t$	=	$r(\sin \varphi \cdot \tan \varphi)/2$
Sagittal Fan Angle, α_s	=	$D/S'_s = 2D(\cos \varphi)/r$
Tangential Fan Angle, α_t	=	$D(\cos \varphi)/S'_t = 2D/r$

Location of each heliostat relative to the tower-receiver determines the focal distance or slant range, d. A slant range equal to r/2 produces the minimum circle of confusion[9] which is a section thru the image forming fan of rays that is

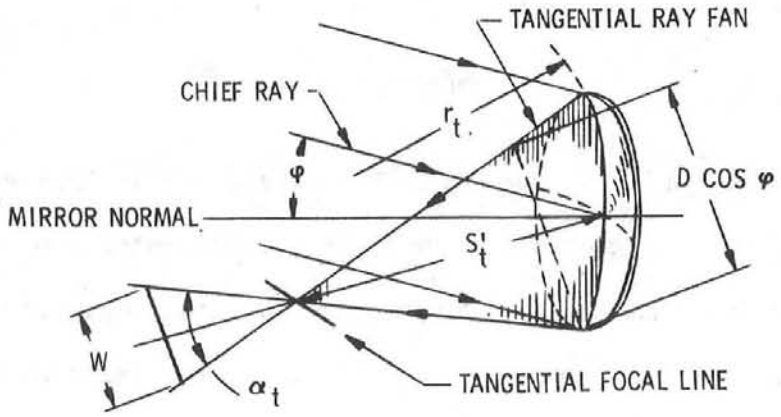

(a)

$1/S + 1/S'_t = 2/(r \cos \varphi)$

CODDINGTON EQUATION FOR LOCATION OF TANGENTIAL FOCUS[8]

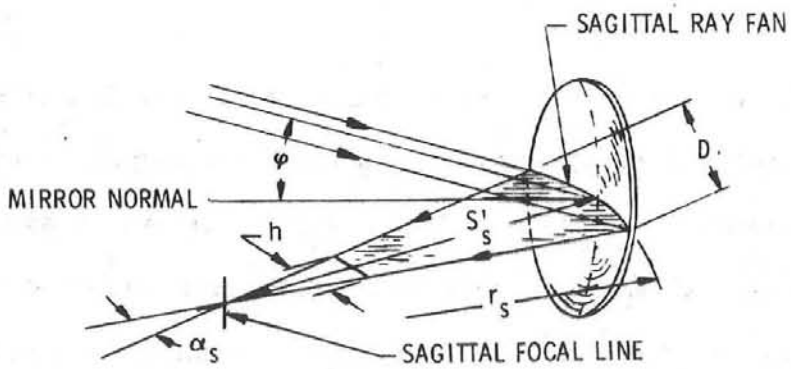

(b)

$1/S + 1/S'_s = 2 \cos \varphi / r$

CODDINGTON EQUATION FOR LOCATION OF SAGITTAL FOCUS[8]

FIG. 5 GEOMETRY TO DESCRIBE THE PARAMETERS FOR ANALYTICAL MODEL

circular in form with equal diameters. Images from the lab-heliostat were measured at a slant range equal to r/2. Of special interest is the heliostat's depth of focus and an equation for depth of focus is given in Appendix A. The first order approximation to the magnitude of image height, h, at a given slant range is given by

$$h = \alpha_s (S'_s - d) + \beta_s d \qquad (1)$$

$$= 2D \sin^2 (\varphi/2) + \beta_s r/2$$

where β_s is the angle subtended by the sun. The first term of this expression describes the contribution to image-height from axially collimated rays while the second term describes the contribution from the non-axially collimated rays produced by the finite angular size of the sun. Similarly the image width, w, is given by

$$w = \alpha_t (d - S'_t) + \beta_s d \qquad (2)$$

$$= 2D \sin^2 (\varphi/2) + \beta_s r/2$$

These analytical expressions predict the measured image heights and widths produced by the laboratory facet and heliostat mock-ups with considerable accuracy over the angular range of 60 degrees as shown in Fig. 6. While spherical and comatic aberrations exist, they are for the most part overwhelmed and concealed by the large astigmatic effects at the focal ratios of interest. Although equations 1 and 2 are of a general nature we will discuss throughout this report the image size produced by heliostat dimensions except where noted. To the first order the linear image dimension, h or w, provides the calculated area of the image at the tower-receiver and thus predicts power performance. Rearranging terms in Eq. 1 the dimensionless ratio of aberrated sun image to ideal sun image, $h/(\beta_s d) = [2 \sin^2 (\varphi/2)/(\beta_s F_r)] + 1$, is plotted in Fig. 7 as a function of the incidence angle, φ, for several focal-ratios, $F_r = d/D$. This plot is used later for determining the minimum focal-ratio and thus maximum size for a heliostat at a given location.

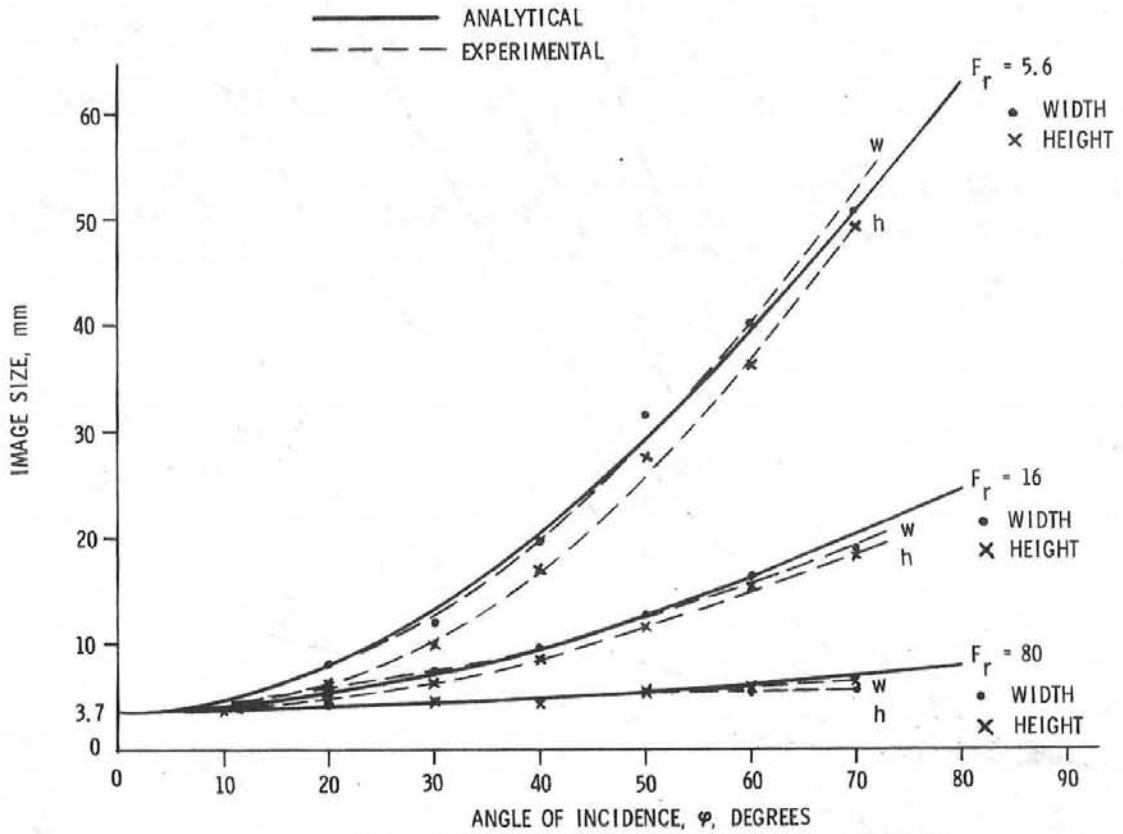

FIG. 6 COMPARISON OF EXPERIMENTAL LABORATORY MEASUREMENTS WITH ANALYTICAL PREDICTIONS AS A FUNCTION OF ANGLE OF INCIDENCE. ON AXIS LABORATORY IMAGE DIAMETER OF SIMULATED SUN EQUALS 3.7 MILLIMETERS.

Generation of a Toroidal Heliostat Surface

Fig. 8 shows the location of simulated sun images from discrete facets of the laboratory-heliostat at values of φ = 40 and 50 degrees. Note that the corner facets define the boundary of the image as produced by a fully illuminated laboratory-heliostat as shown in Fig. 4 at φ = 40 and 50 degrees. Similarly, a field heliostat behaves like a single spherical surface having a focal length equal to that of the individual facet. At large angles of incidence heliostat images are correspondingly large. Optimum image reduction can only be accomplished by individually aligning the facets of a heliostat for each operational angle of incidence which changes with sun position. For any angle of incidence the individual facets of a heliostat may be aligned to superpose the individual facet images to a

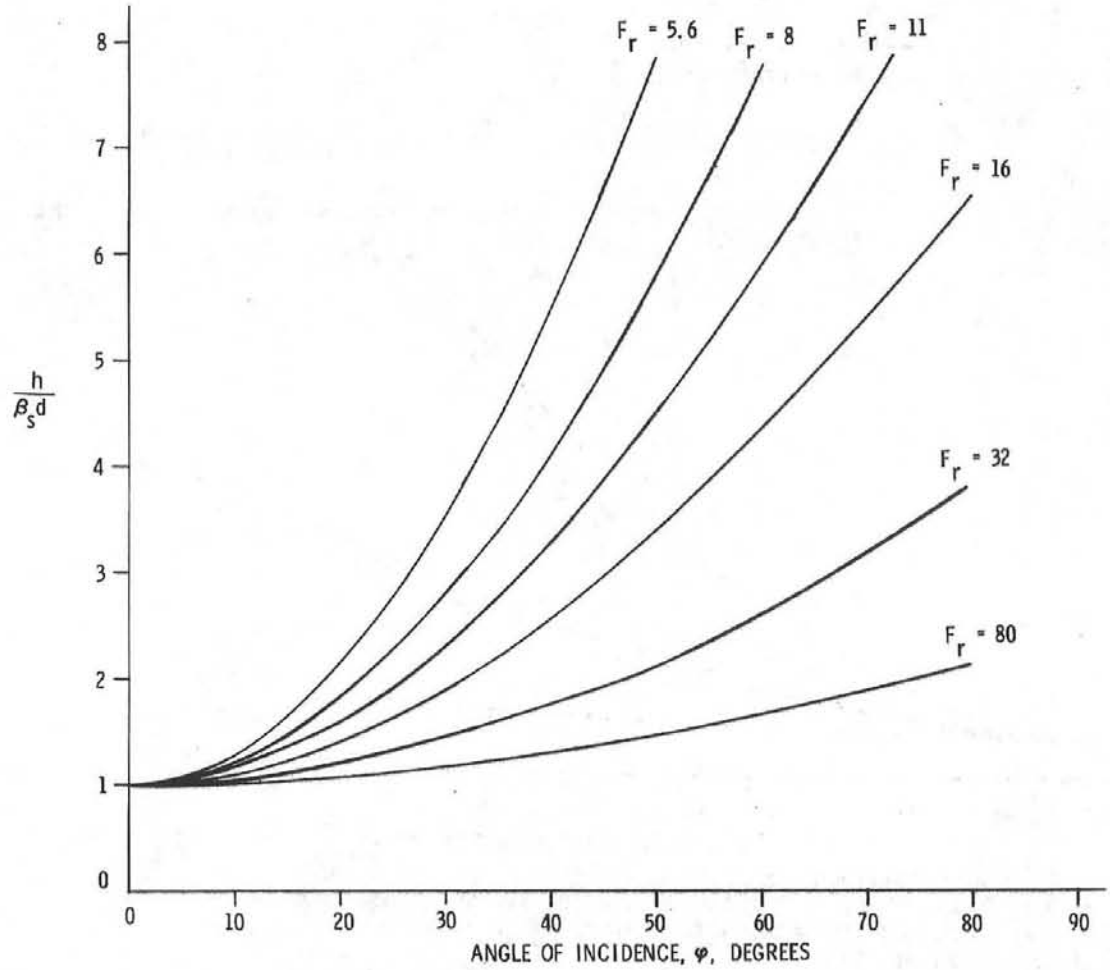

FIG. 7 ABERRATED IMAGE RATIOS PRODUCED BY AN OFF AXIS CONCAVE MIRROR AS A FUNCTION OF ANGLE OF INCIDENCE

common centroid, i.e., to the image from the heliostat's center facet. A heliostat so aligned is here defined as a pre-aligned heliostat. The slope angles at the centers of the facets of such a heliostat are tangent to an imaginary toroidal surface, i.e., a surface whose orthogonal radii are not equal. In effect the heliostat approximates a toroidal Fresnel mirror even though the individual facets are spherical. Examination of such a surface is of interest because this form of heliostat may be used to track the sun at the STTF. A heliostat is pre-aligned when $S'_s = S'_t$ for a given $\bar{\varphi}$ where $\bar{\varphi}$ is the angle of incidence at pre-alignment. Optimization of the toroidal shape is obtained when

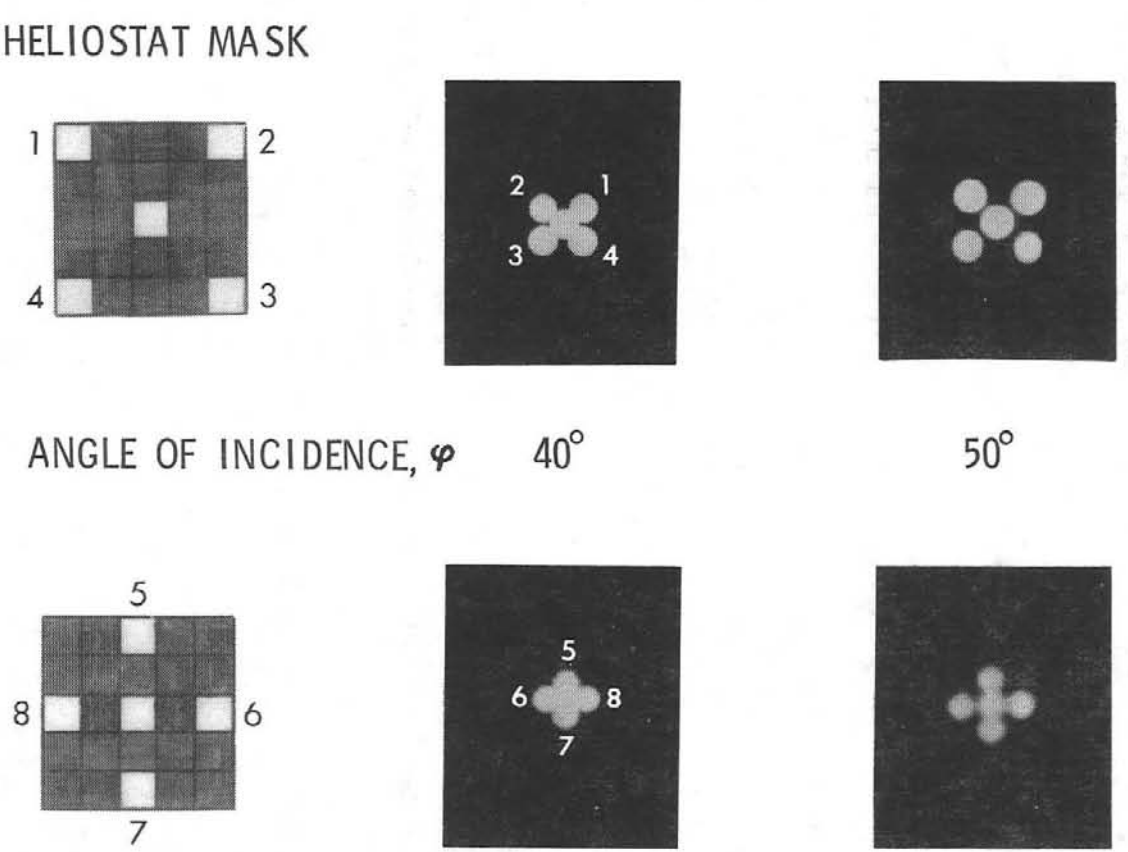

FIG. 8 LOCATION OF SIMULATED SUN IMAGES AS PRODUCED BY SPECIFIED FACETS OF LAB-HELIOSTAT

$$r_t = r_s \sec^2 \bar{\varphi}$$

where r_t amd r_s are the respective tangential and sagittal radii and where r_t lies in the incident plane. When $\bar{\varphi} = 0$, r_t equals r_s and the heliostat surface is now symmetrical about its center. When a heliostat is pre-aligned for $\bar{\varphi} \neq 0$, the angle, ψ, must be specified, where ψ defines the projection of the plane of incidence onto the heliostat surface. The angle ψ is used to reference the non-symmetrical surface of the pre-aligned heliostat and its significance is discussed later.

Consider a pre-aligned heliostat such that the sagittal and tangential conjugates are equal at a chosen slant range.

$$\begin{aligned} S'_s &= d & \text{and} \qquad S'_t &= d \\ S'_s &= (r_s \sec \bar{\varphi})/2 = d & S'_t &= (r_t \cos \bar{\varphi})/2 = d \\ r_s &= 2d \cos \bar{\varphi} & r_t &= 2d \sec \bar{\varphi} \end{aligned} \tag{3}$$

Since we have expressed the toroidal radii as a function of slant range and $\bar{\varphi}$ the equations for the sagittal and tangential conjugates of a pre-aligned heliostat are given by

$$\begin{aligned} S'_s &= d \cos \bar{\varphi} \sec \varphi \\ S'_t &= d \sec \bar{\varphi} \cos \varphi \end{aligned} \tag{4}$$

These values are substituted in Eqs. 1 and 2 to obtain the image heights and widths for a pre-aligned heliostat.

$$\begin{aligned} h &\simeq \alpha_s S'_s \left|1 - \frac{d}{S'_s}\right| + \beta_s d = D\left|1 - \frac{d}{S'_s}\right| + \beta_s d = D\left|\frac{\cos \bar{\varphi} - \cos \varphi}{\cos \bar{\varphi}}\right| + \beta_s d \\ w &\simeq \alpha_t S'_t \left|\frac{d}{S'_t} - 1\right| + \beta_s d = D \cos \varphi \left|\frac{d}{S'_t} - 1\right| + \beta_s d = D\left|\cos \bar{\varphi} - \cos \varphi\right| + \beta_s d \end{aligned} \tag{5}$$

When the operational angle of incidence, φ, equals the angle of incidence at pre-alignment, $\bar{\varphi}$, then the image size is minimum and equal to $\beta_s d$. Eq. 5 is shown in Fig. 9 where the aberrated image-ratio is plotted for a focal ratio of 16 and four values of $\bar{\varphi}$. Remember that the image plane modeled here is normal to the chief-ray and that image height and width are respectively oriented perpendicular and parallel to the operational incident plane. The operational incident plane, which is defined by the centers of the sun, heliostat and tower receiver-aperture, rotates about the line from the center of the heliostat to the center of the receiver-aperture as the sun position changes throughout the day. Incident plane rotation in combination with the projection of the receiver-aperture onto the image plane finally describes that part of the image spot that will be utilized. Application of Fig. 9 is restricted to the special case in which the radius r_t of the toroidal-heliostat-surface rotates with the operational incident plane. Additionally, Fig. 9 describes the case in which the individual facets are toroidal and rotate with the operational incident plane. Even with these restrictions Eq. 5 gives a fair approximation (predicted image sizes smaller than true values) for images produced by heliostats having spherical facets. While problems of orientation and facet shape are ultimately important they are not included at this point for model simplicity.

Analysis of an Existing Heliostat Array

Using the linear dimensions of an image produced by a given heliostat pre-aligned for $\bar{\varphi} = 0$, (h and w are functions only of D and φ, i.e. Eq. 5 reduces to Eqs. 1 and 2) prediction of image size is easily made by determining the angles of incidence at which a tracking heliostat operates as a function of the hour of day for a specified day. Each heliostat gives a unique image signature with both day and time of day.

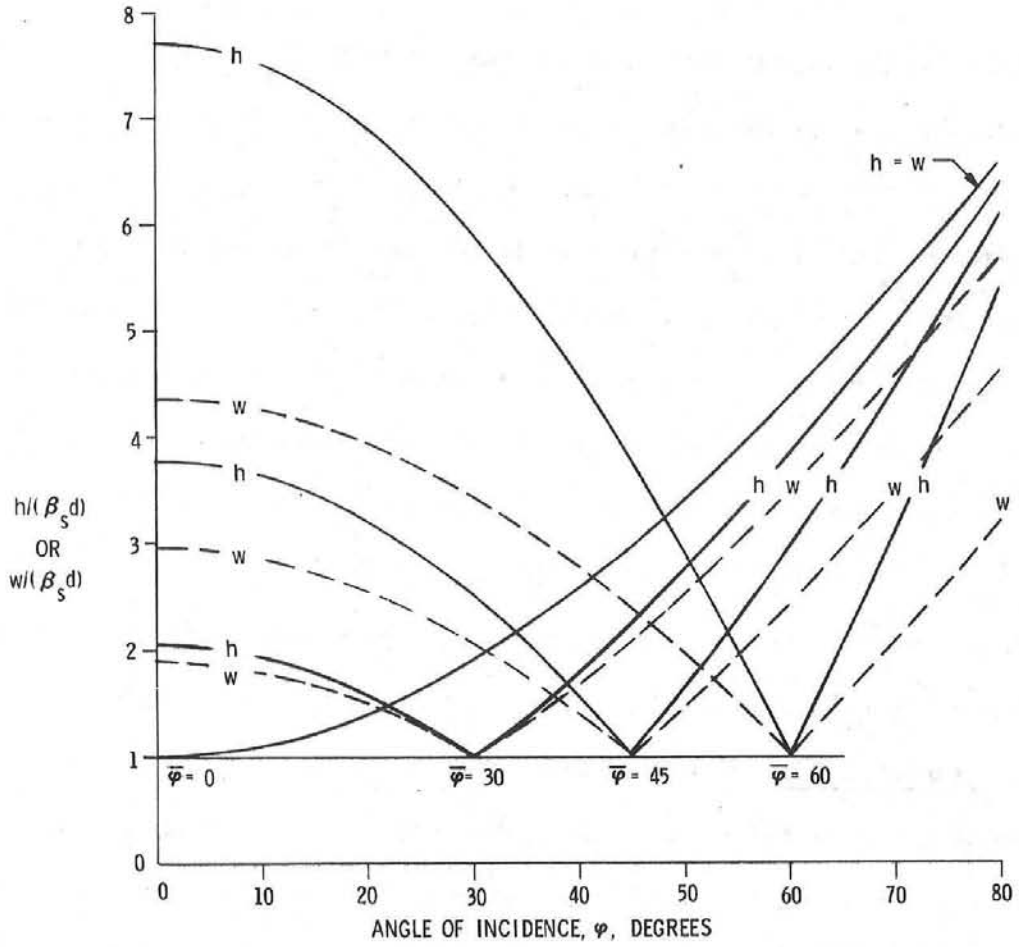

FIG. 9 ABERRATED IMAGE RATIOS FOR PRE-ALIGNED HELIOSTAT WITH $F_r = 16$ AS A FUNCTION OF ANGLE OF INCIDENCE

Figure 10 shows the path of the sun across the sky for the equinox and the summer and winter solstices. These are the mean and the extremes of the solar paths seen from the heliostat array. Each heliostat must operate in such a way that the incident radiation is always reflected to the receiver. Therefore, the direction and slant range to the target from the heliostat are constant for each heliostat and depend only on the heliostat-target geometry. The line from the center of the sun to the center of the heliostat and the line from that center to the target define a plane, the plane of incidence, which must also contain the normal to the optical surface at that point. The normal must bisect the angle between the incident and reflected rays in order that the law of reflection be

obeyed. The angle between the incident ray and the surface normal is the angle of incidence used through this report.

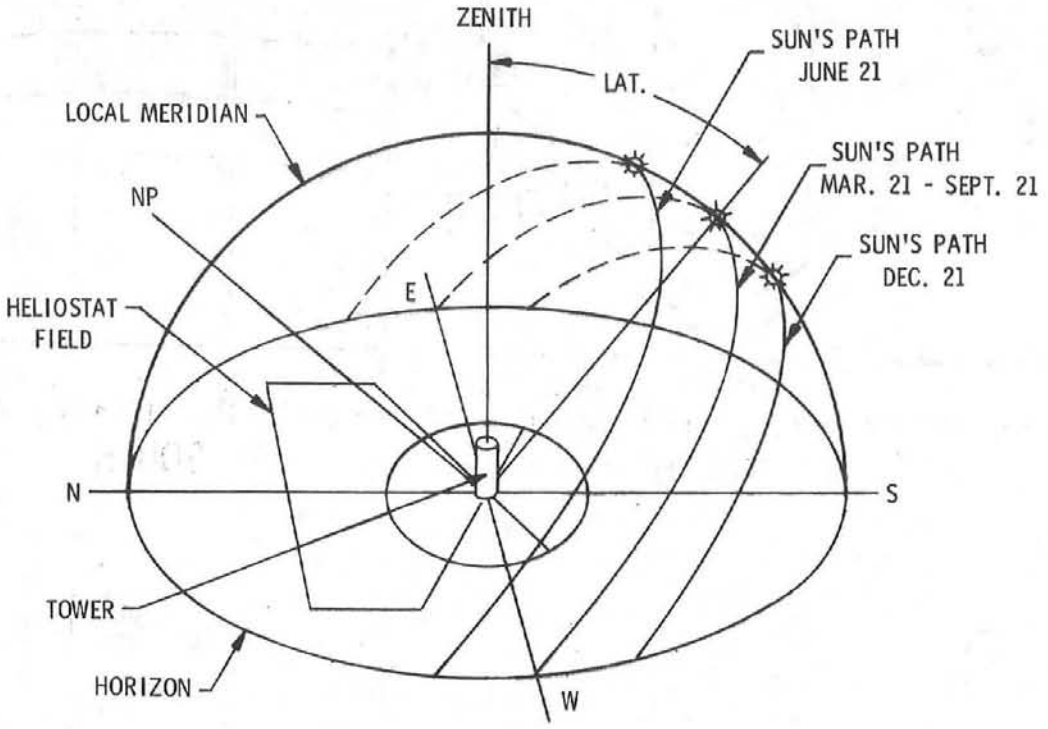

FIG. 10 PATH OF SUN RELATIVE TO HELIOSTAT FIELD & TOWER

A computer program was written to calculate and plot the incident angles for representative heliostats in the array for the solstices and equinoxes.

The plots are for latitude	35° 7' (Albuq., N.M.)
Declinations	±23.433°, 0
Local Solar Times	6 to 18 hrs.

The errors caused by using local solar time shift the curves slightly along the time axis but do not alter their shape. The error from ignoring the change in declination during the day would not exceed 0.1 degrees. Fig. 11 shows the envelope of incident angles for representative heliostats at a constant slant range. Note, a negative coordinate is used to specify the opposite axis, i.e., -N=S and

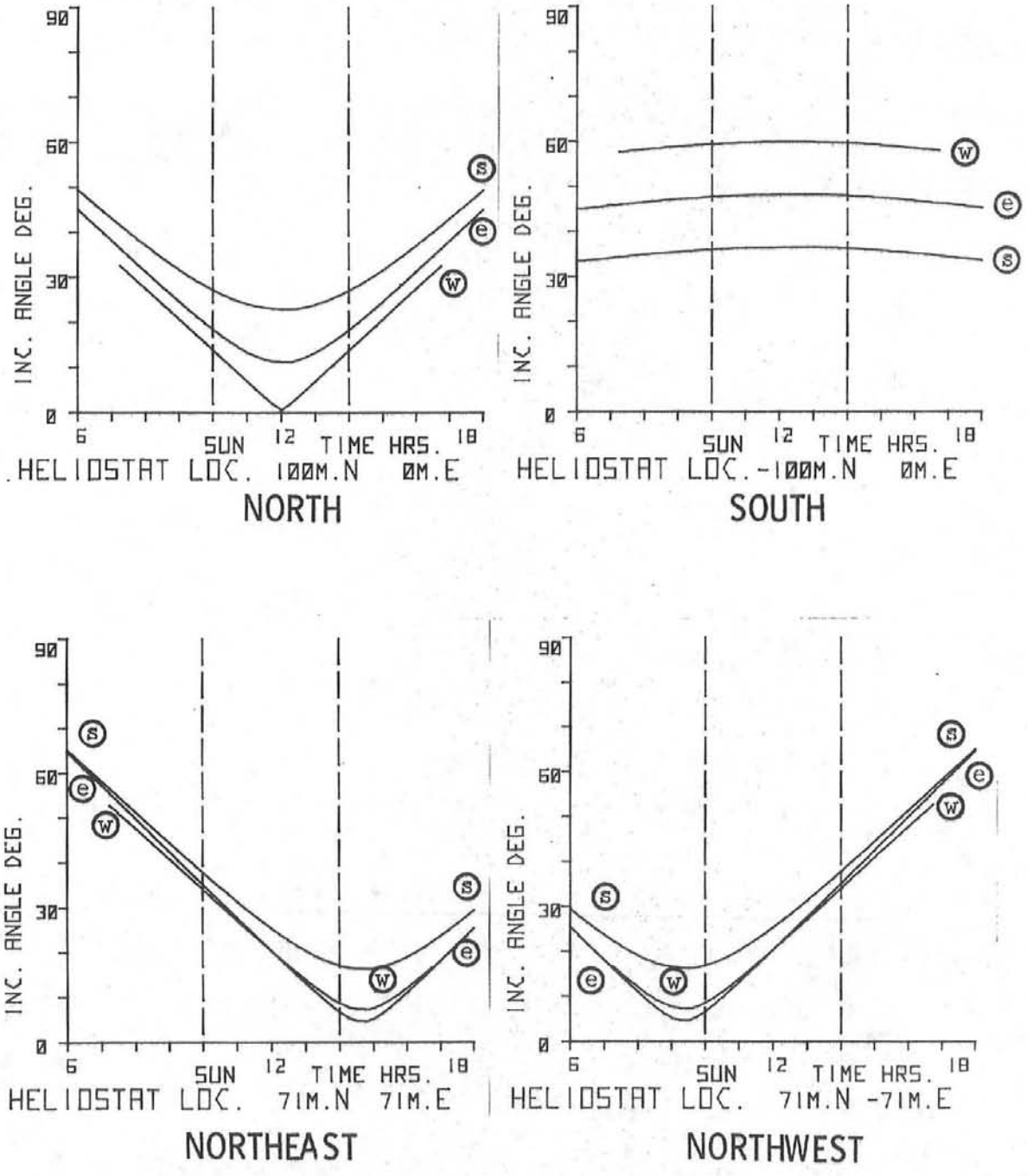

FIG. 11 INCIDENT ANGLE VS. TIME FOR SELECTED CONSTANT SLANT RANGE HELIOSTATS - TOWER RECEIVER IS 62.3 m HIGH

Ⓦ, Ⓢ and Ⓔ are the winter and summer soltices and equinox. Attention is called to the expected incident-angle-symmetry about noon as shown in Fig. 11 for heliostats on the North-South axis. While this symmetry is maintained on the South axis the daily range of incident-angles is minimum. For heliostats on a Northeast and Northwest axis there is no 1200 hour symmetry; however, the envelope of incident angles are 'mirror-images' of each other and in this sense symmetry does exist. While Fig. 11 gives an overview for incident angles as a function of sun time it is necessary to obtain this data for each specific heliostat to be evaluated. For example, angles of incidence vs sun time for heliostat #18 located in STTF field A for a one-megawatt thermal test target, with an assumed projected area of 1 m^2, are shown in Performance Table I and the listed linear dimensions are calculated from Eqs. 1 and 2. The percent of image area collected is found by dividing the projected area of a given receiver-aperture (as seen by the heliostat) by the calculated image area, (h•w). The percent of the power collected approximately equals the triple product of the percent image area collected, the cosine of the angle of incidence (which accounts for the effective or projected heliostat area as seen from the receiver) and the mirror's assumed reflection coefficient of 0.9. The primary reason for including this table is to show methodology. Based on utilizing the whole of heliostat field A (Fig. 1) which could collect approximately 2.25 thermal megawatts at normal incidence, (assumed insolation of 0.8 kW per m^2), it is not necessary to conduct a detailed analysis to conclude that the one megawatt thermal test is realizable.

A similar analysis is made for a four-megawatt thermal test in which a receiver rated at five-megawatts is located approximately 62.3 meters high above the heliostats. Fig. 12 gives the angle of incidence vs. sun time for selected heliostats and Fig. 13 gives predictions for STTF power-collection at the target, 2.65 m x 2.65 m,

Table I

Heliostat #18 June 21st. Projected Area of Receiver Aperture - 1 m^2

Sun Time Hrs.	Angle of Incidence φ, degrees	Linear Dimension h=w, meters	Image Area Collected, %	Total Power Collected, %
6	36.8	1.66	36	26
7	29.9	1.26	63	49
8	23.3	0.96	100	83
9	17.2	0.73	100	86
10	12.3	0.60	100	88
11	10.6	0.56	100	88
12	13.4	0.63	100	88
13	18.7	0.78	100	85
14	25.1	1.03	94	77
15	31.7	1.36	54	41
16	38.6	1.78	32	23
17	45.4	2.25	20	13
18	52.3	2.80	13	7

as provided by heliostat Nos. 18, 105, 141 and 142, (approximate locations on Fig. 1). Heliostat #18 is near the North axis and has a minimum slant range of $\simeq$ 66 m. Heliostat #105 is, we believe, representative of those at about mid-field and has a slant range of $\simeq$ 152 m. Heliostat numbers 141 and 142 are at the extremes of the field with #141 on the northwest corner and #142 near the North axis. They have respective slant ranges of $\simeq$ 220 and 196 meters. Fig. 13 shows power received from selected heliostats with the interval between circles on each curve indicating the time interval during which the image size is equal to or less than the size of the receiver-aperture. Reduction in power during this interval is due solely to the change of heliostat projected-area as seen by the receiver.

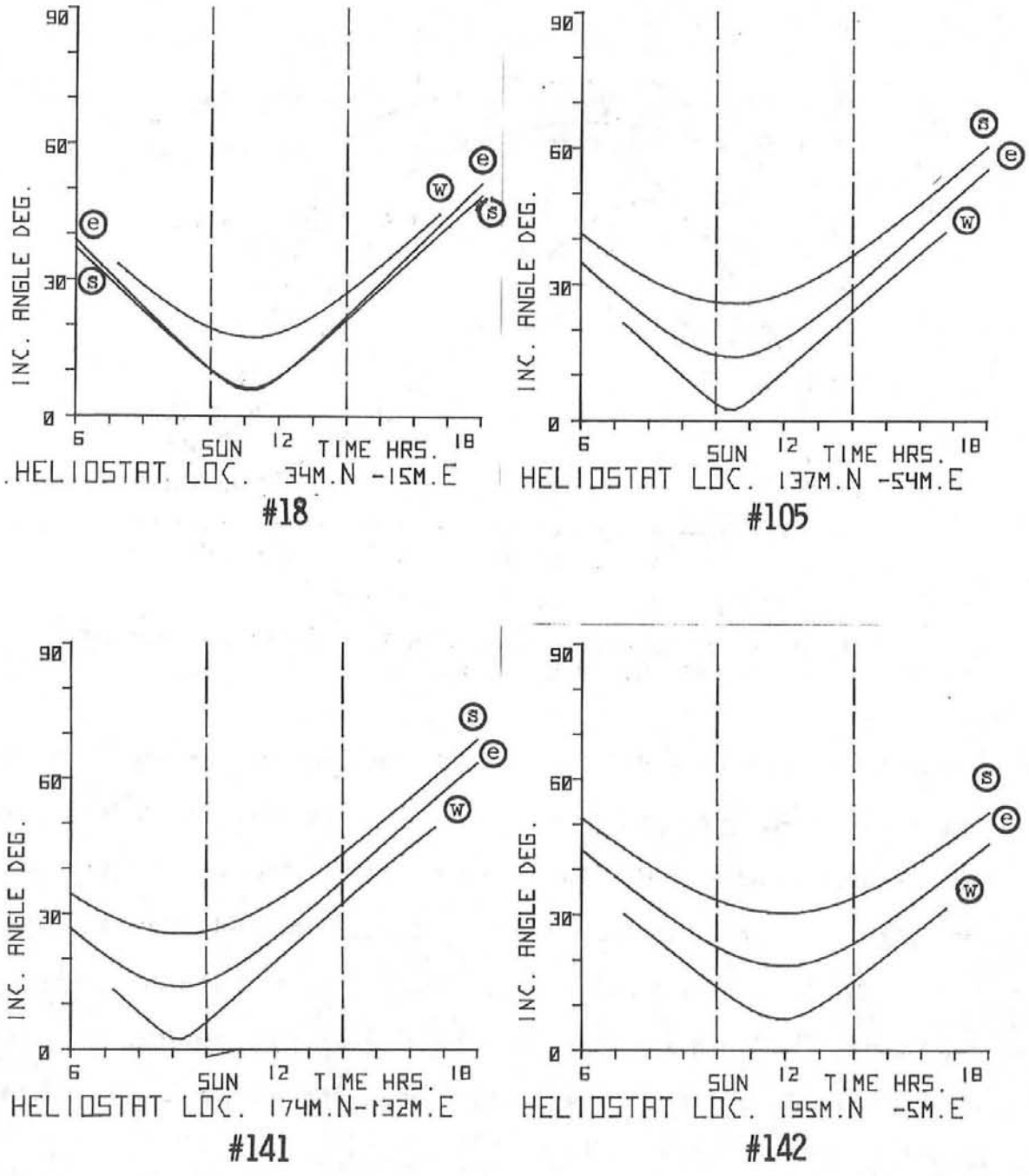

FIG. 12 INCIDENT ANGLE VS. TIME FOR SELECTED HELIOSTATS - TOWER RECEIVER IS 62.3 m HIGH

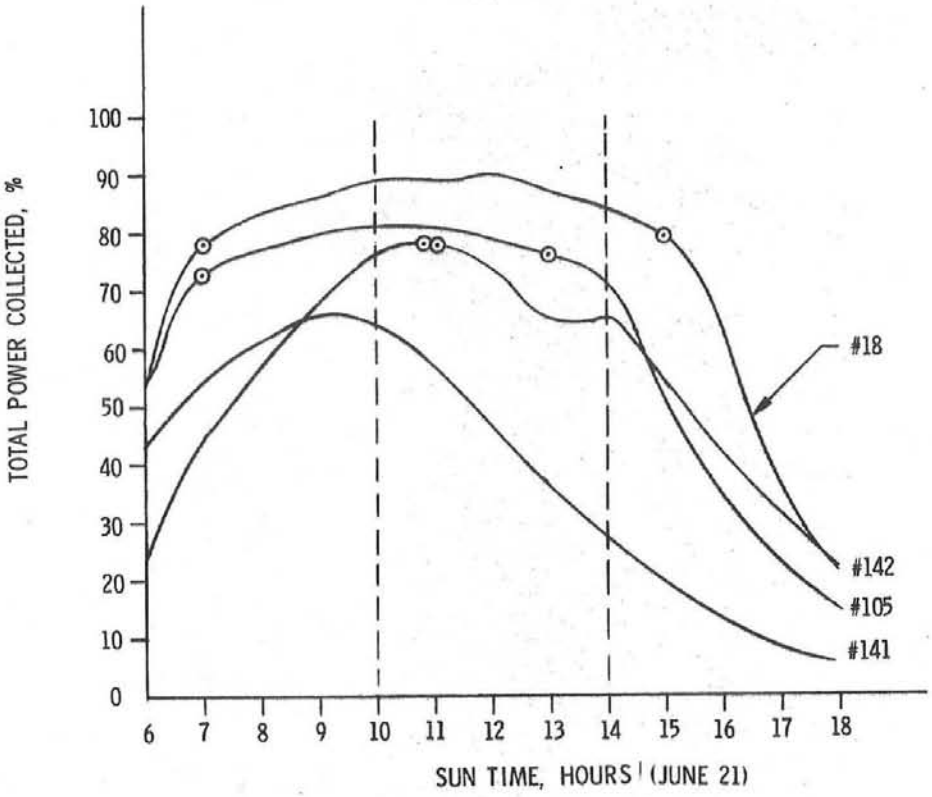

FIG. 13 POWER FROM SELECTED HELIOSTATS IN STTF NORTH FIELD VS. SUN TIME
RECEIVER APERTURE IS 2.65 m x 2.65 m

Reduction in total power on either side of this time interval is due both to continued image growth and projected area effects. To differentiate these effects or to find the projected area of the receiver-aperture see Appendix B. Note that there are no circles indicated for the curve of heliostat #141, Fig. 13, because at no time is the image area less than the projected area of the receiver-aperture. Remember, these predictions are based on perfect optics, no toroidal surfaces, constant radiance across the sun's disk, no atmospheric absorption and no alignment errors.

Clearly the power from heliostat numbers 141 and 142 during the specified operating interval (10 AM to 2 PM) is less than ideal and drastic power reduction occurs when the operating interval is extended. As is shown later in the development this simple model, Eqs. 1 and 2, predicts a larger power loss over the 10 AM

to 2 PM interval and, a lower power loss outside this time interval compared to what is realizable. However, since the heliostat North field (A and B) is capable of collecting an average total power of 6.4 megawatts at normal incidence it is concluded (from the optical aberration analysis) that a four megawatt thermal test is realizable even though many heliostats will not be optically operating at full efficiency, i.e. image sizes larger than receiver. The generous thermal power deratings and limited duty cycle (10 AM to 2 PM) available to STTF cannot be tolerated at an electric power facility. The economics of electric power generation must be predicted on a full sun day and on a large surrounding heliostat-field which in turn results in large angles of incidence for the collecting optics at the earlier and later hours of the day. To increase the total power collected over a full sun day, daily adjustments of the heliostat surface, e.g. aligning facets to a toroidal locus, are necessary.

Design Consideration for a Heliostat Array

At least two general types of error caused by heliostat and facet deformation in the field should be considered. Both errors reduce the power received at the tower-receiver. Consider an angular error, γ_f, generated by facet defocusing due to structural deflection, and/or mechanical misalignment to the heliostat-frame and random heliostat-frame deformations. These errors associated with γ_f are postulated as symmetrical errors that simply cause the image size to increase relative to the centroid of the optimum image. There is another error γ_p generated by heliostat pointing which only translates the given image-centroid to a new position. It is difficult to access this latter error relative to a permissable error for aberrated image-growth. For example, if γ_p places the image-centroid of minimum size at the periphery of the receiver-aperture then astigmatic image growth neither increases nor decreases the energy collected until radial growth of the image exceeds

the enclosed aperture of the receiver. On the other hand if the value of γ_p places the image-envelope of minimum size inside but tangent to the receiver-aperture then the astigmatic image growth must be zero to maintain the initially collected energy. Limiting ourselves to errors of the first kind, γ_f, a function for permissable astigmatic image growth is given by

$$\boxed{h/(\beta_s d)} = \frac{C-2\gamma_f d}{\beta_s d} \qquad (6)$$

where C is the linear dimension of the receiver-aperture and where $h = C-2\gamma_f d$. The value of $2\gamma_f d$ is the effective loss in size of the receiver-aperture. Fig. 14 shows this relationship for several assigned values of γ_f in radians as a function of slant range, d. An undesirable ratio of less than unity shows that the linear dimension of the tower-receiver is less than the minimum image of the sun. Given the slant range and estimated γ_f-value for a proposed heliostat location, a value of $\boxed{h/(\beta_s d)}$ is obtained which in turn is used for entry to Fig. 7 together with heliostat angle of incidence data from Fig. 12. Although Fig. 7 describes the general case for a spherical surface and applies equally well to either a facet or heliostat we consider here only the case for a heliostat. The equation defining Fig. 7 then provides the minimum focal-ratio commensurate with permitted image growth. Finally, this focal-ratio divided into the slant range establishes the maximum linear dimension, D, for the heliostat. The basic lesson here is that small slant ranges should utilize large heliostats and conversely large slant ranges should utilize small heliostats. In the limit, as $\beta_s d_{max.} \rightarrow C$ the size of the heliostat approaches zero when the incident angle range covers a full sun day. While this limit prescribes an unacceptable operational condition, it does verify a need for a heliostat having adjustable facets. One could place all heliostats

at a minimum slant range by locating an array of heliostats on a spherical section whose chordal plane is vertical with the central-receiver at the center of curvature.

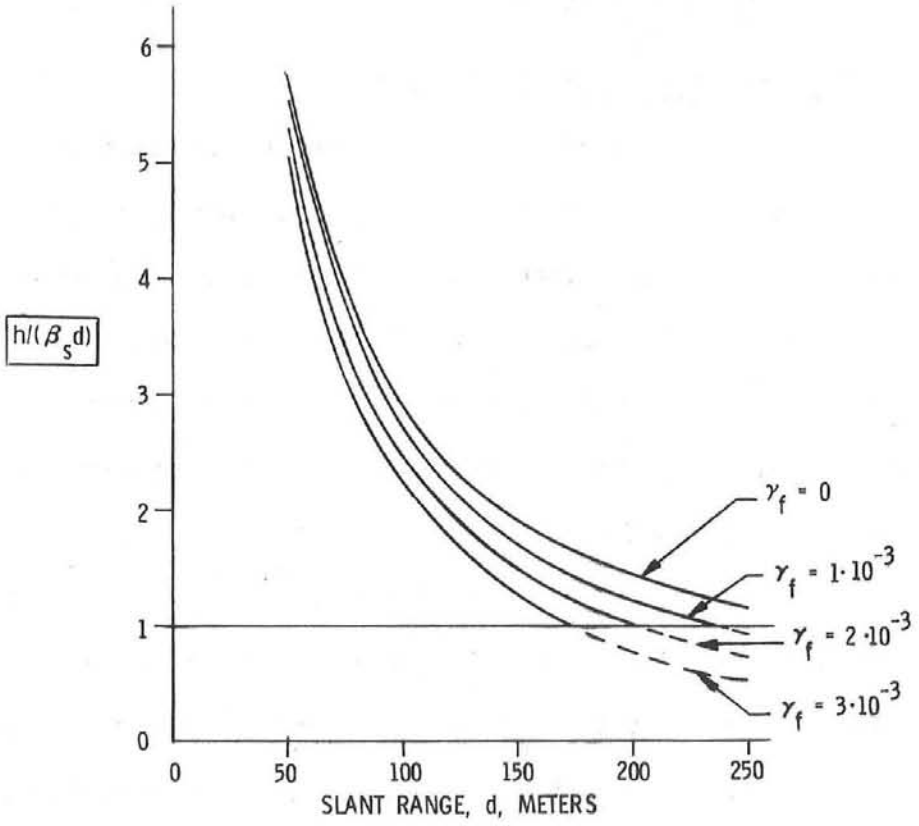

FIG. 14 PERMISSABLE ABERRATED IMAGE RATIO FOR A 2.65 METER RECEIVER AS A FUNCTION OF SLANT RANGE.

There are of course predictive refinements which alter the estimated value for D, e.g., Eq. 5 as plotted in Fig. 9. By choosing an appropriate value of $\bar{\varphi}$ for a heliostat operating over a small incident angle range, the value of $h/(\beta_s d)$ is reduced below the value obtained when $\bar{\varphi} = 0$. However, the value of $h/(\beta_s d)$ increases over the value obtained for $\bar{\varphi} = 0$ when the operating time interval is increased (large incident angles) because the heliostat's toroidal radii are generally

not properly oriented with respect to the operating incident plane. This mis-orientation markedly increases image size. In the final analysis the orientation of the toroidal mirror must be considered in estimating the dimension, D, as well as in calculating the values for h and w.

Orientation and Description for a Toroidal Mirror

A general description is developed for image size as produced by a pre-aligned STTF heliostat. Consider a heliostat frame having individually attached spherical mirrors so aligned to the heliostat frame that the normals at the centers of each spherical facet are normal to an imaginary toroidal locus. This is the condition obtained when a heliostat is pre-aligned at a given angle of incidence. Any toroidal surface may be described by two perpendicular sections of maximum and minimum curvature. Let the directions of the sections correspond to r_t and r_s as shown in Fig. 15 with r_t located in the plane of incidence. The orientation of the toroid is described by the angle ψ. The angle ψ is the angle formed between the heliostat elevation-axis (reference line) and the line, lying in the heliostat frame-plane, which is formed by the intersection of the incident plane at pre-alignment with the heliostat frame-plane. In this discussion the heliostat frame-plane is the plane to which the individual facets are attached. The heliostat elevation-axis is considered to lie in this plane and essentially does. When facing the mirrored heliostat frame-plane the angles ψ and τ are measured counter-clockwise from the right side of the heliostat elevation-axis. Angle τ is the angle formed between the heliostat elevation-axis and the line, lying in the heliostat frame-plane, which is formed by the intersection of the operational incident-plane and the heliostat frame-plane. Determining the angle τ is necessary because it describes the location of the operational incident plane which is used as the reference for calculating image sizes. Therefore, the radius, R_θ, associated with this incident

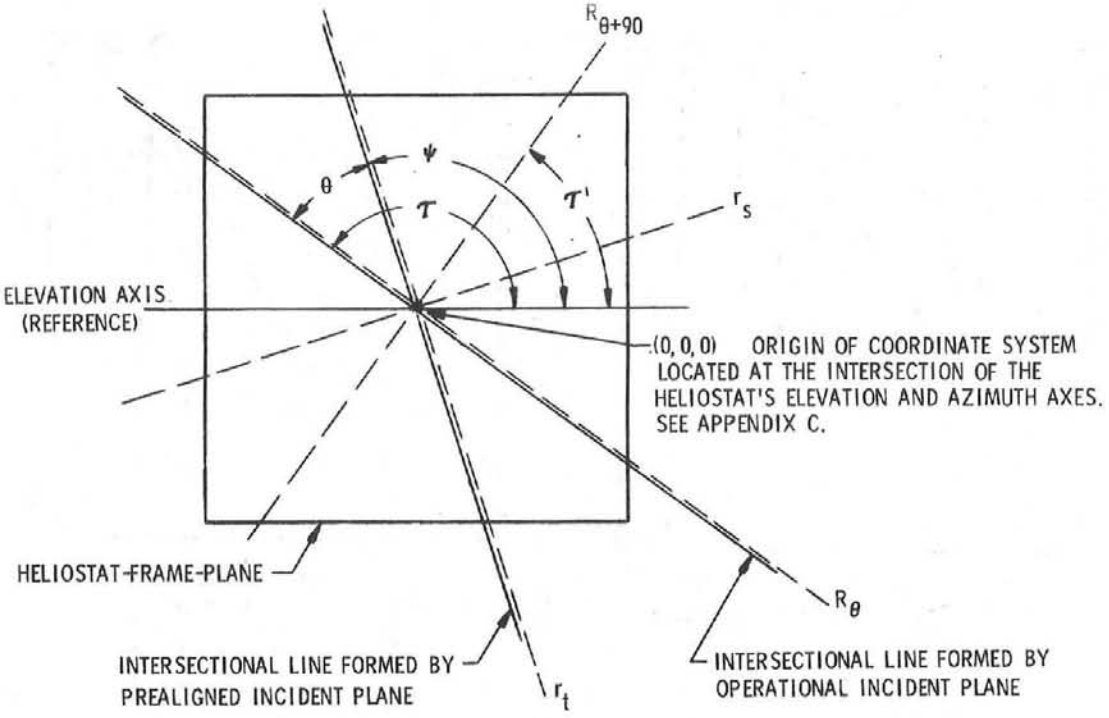

FIG. 15 ORIENTATION-ANGLES AND ORTHOGONAL RADII FOR A PRE-ALIGNED HELIOSTAT

plane location and the orthogonal radius, $R_{\theta+90}$, are required to describe image size. The angle τ' (related to the angle τ) is the angle between the elevation axis, Fig. 15, and the line, $R_{\theta+90}$, lying in the heliostat frame-plane and normal to the operational incident plane. The derivation[10] for τ' is found in Appendix C. Since the vector algebra only allows values for this angle equal to or less than 180 degrees, τ' is positive when the line $R_{\theta+90}$ has a positive slope and τ' is negative when $R_{\theta+90}$ has a negative slope. Therefore, $\tau = |90 + \tau'|$ and the limit, $180 \geq \tau \geq 0$, is imposed. This arithemetic convenience does in turn generate a striking function in Fig. 16 which gives the angle τ as a function of sun time for heliostat numbers 141 and 142. Large angles for τ at early morning and small angles of τ for evening are noted. If at the vertical discontinuities the morning function is shifted down and the evening function is shifted up to spline these functions then a single continuous function is obtained and conforms to

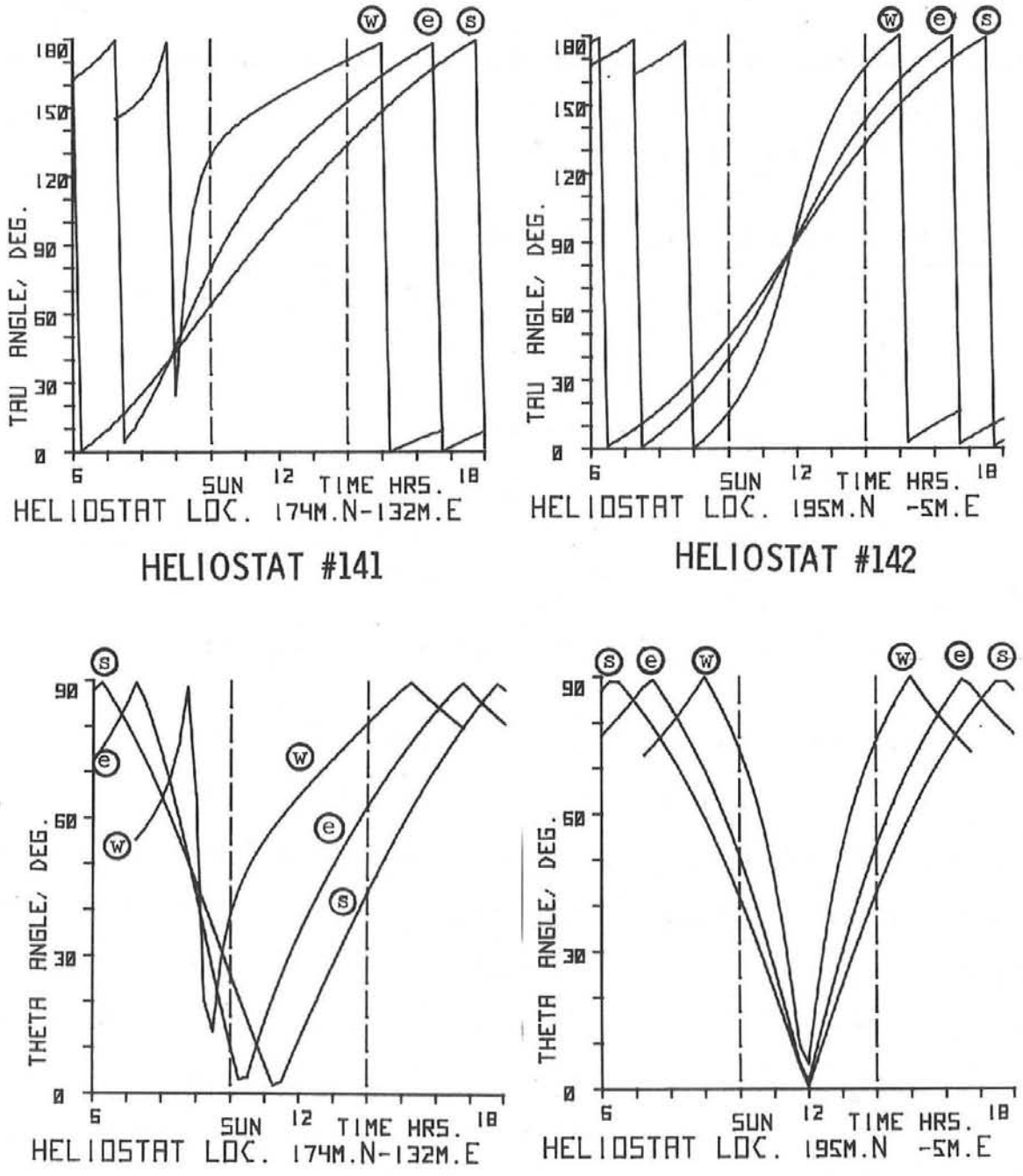

FIG. 16 ORIENTATION ANGLES VS. SUN TIME FOR SELECTED HELIOSTATS - TOWER TARGET IS 62.3 m HIGH

expected physical reality for the total daily angular range. For heliostats lying on the North and South axes the total angular range is maximum and approximately equal to 180°. Heliostats on the East-West axis have the minimum angular range which is always less than 90°.

In field practice the angles φ and τ at a specified sun time are used to define the angles $\bar{\varphi}$ and ψ for pre-alignment. In principle pre-alignment of the heliostat is obtained in the field with the use of a laser interrogating a selected heliostat. Both laser and heliostat are computer programmed to respectively simulate the position of the sun at a given time for a specified day and the position of the heliostat which would locate the image of the sun at the center of the receiver-aperture. For the specified sun position the individual facets are theoretically aligned to superpose all images at the image of the center facet.

The absolute difference between the angles specified, $|\psi-\tau|$, defines the angle θ which is a function of sun time and which is the angular mis-orientation between the operational incident plane and the pre-aligned incident plane. Angle θ, Fig. 16, is the important parameter because it defines the radius R_θ and its orthogonal radius $R_{\theta+90}$ which respectively lie parallel and perpendicular to the operational incident plane for the angle ψ that applies to the orientation of the pre-aligned heliostat. From a general theorum due to Euler[11] we may write

$$R_\theta = r_s \sin^2\theta + r_t \cos^2\theta \qquad (7)$$

$$R_{\theta+90} = r_s \cos^2\theta + r_t \sin^2\theta$$

where r_s and r_t are the radii prescribed by the pre-alignment angle $\bar{\varphi}$. Remember that although the pre-aligned heliostat has concave spherical mirrors the toroidal radii defining the surface of the heliostat are defined by the slope angles at the

centers of the individual facets. Visualize the very small mirror area perpendicular to the normal of each individual facet. Image sizes produced by these small and essentially flat mirrors which are tangent to R_θ and $R_{\theta+90}$ can be described by equations 1 and 2. Rearranging equations 1 and 2 we have

$$h = (D-\overline{D})\left|\left(1 - \frac{d}{S'_s}\right)\right| + \beta_s d$$

$$w = (D-\overline{D})(\cos\varphi)\left|\left(\frac{d}{S'_t} - 1\right)\right| \beta_s d$$

where $\overline{D}$ is the dimension of a single facet and the quantity $(D-\overline{D})$ is the distance between the centers of the heliostat boundary facets. We then have remaining one spherical facet (i.e. two one-half facets from the boundary facets) that require modeling. Since the first term of primary equations 1 and 2 model the point source or axial astigmatic aberrations we can now write the following inclusive function for a heliostat comprised of concave spherical facets:

$$h = (D-\overline{D})\left|\left(1 - \frac{d}{S'_s}\right)\right| + 2\overline{D}\sin^2(\varphi/2) + \beta_s d$$

$$w = (D-\overline{D})(\cos\varphi)\left|\left(\frac{d}{S'_t} - 1\right)\right| + 2\overline{D}\sin^2(\varphi/2) + \beta_s d$$

where the first additive term describes image aberration produced by the major dimension of the heliostat regardless of the facet shape, (i.e. flat, spherical or toroidal), where the second term for the case treated here describes the image aberration produced by a spherical facet and where the last term accounts for the finite size of the sun. From the Coddington equations we obtain:

$$S'_s = R_{\theta+90}(\sec\varphi)/2 \qquad S'_t = R_\theta(\cos\varphi)/2$$

Substituting for R_θ and $R_{\theta+90}$ from above and remembering from Eq. 3 that $r_s = 2d$ $\cos\bar{\varphi}$ and $r_t = 2d \sec\bar{\varphi}$ we finally resolve

$$h \simeq (D-\bar{D})\left|1-\cos\varphi(\cos\bar{\varphi}\cos^2\theta + \sec\bar{\varphi}\sin^2\theta)^{-1}\right| + \tag{8}$$

$$2\bar{D}\sin^2(\varphi/2)+\beta_s d$$

$$w \simeq (D-\bar{D})\left|(\cos\bar{\varphi}\sin^2\theta + \sec\bar{\varphi}\cos^2\theta)^{-1} - \cos\varphi\right| + \tag{9}$$

$$2\bar{D}\sin^2(\varphi/2) + \beta_s d$$

These expressions now provide the complete description for dimensions, h and w, which are measured perpendicular and parallel to the operational incident-plane for a heliostat consisting of concave spherical facets.

As an example let us calculate the images produced by heliostats, Nos. 141 and 142, having respective slant ranges of 220 and 196 meters, and aimed at the 5 megawatt Martin-Marietta receiver. If we assume heliostat numbers 141 and 142 were pre-aligned at noon on the summer soltice then from Fig. 12 the respective values of $\bar{\varphi}$ are 35 and 32 degrees. The arbitrary value of $\psi = 90$ degrees was assigned to both heliostats. While any arbitrary values for $\bar{\varphi}$ and ψ may be chosen, in field practice, the angles φ from Fig. 12 and τ from Fig. 16 at a specified sun time are used to define the angles $\bar{\varphi}$ and ψ for pre-alignment. Since the values of φ and $\theta = |\psi-\tau|$ for these heliostats are now available, (Figs. 12 & 16), Eqs. 8 and 9 may be used to calculate values for h and w for each heliostat operating in three possible modes:

A) non-aligned or spherical, $\overline{\varphi} = 0°$ and $\theta = 0°$ (available at STTF)

B) pre-aligned at $\overline{\varphi}$ (available at STTF)

C) pre-aligned at $\overline{\varphi}$ plus rotational tracking, $\theta = 0°$ (not available at STTF)

Values for h and w for heliostat Nos. 141 and 142 are found in Figs. 17 and 18. Orientation of the image envelope relative to the receiver-aperture is not considered. Losses here would further decrease calculated power limits, i.e., losses would be larger than those calculated. Unequivocably, a minimum average image size results when the heliostat is pre-aligned and rotational tracking is provided, (mode C). The choice between performance from heliostat modes (A) and (B) is rather complicated and depends upon the optimization criterion chosen, operating time desired and locations of individual heliostats.

Conclusions

Clearly the present STTF design for optical collection and receiver size has severe operational limitations if it is scaled and considered a proto-type for the economic production of electric power, such as, the proposed Barstow, Calif. Solar Tower Electric Facility. Excluding rotation of the heliostat frame about the normal to the center facet and making individual facets toroidal and rotational about their normals, there are only four possible methods for producing an image size compatible with the receiver-aperture size.

1) Reduce linear dimension, D, of the heliostat. Reduction of the linear dimension D of a heliostat may be accomplished by doing the obvious but alternatively, by maintaining the relatively large heliostat frame but having individual facets continuously tracking the sun by programming or by auxiliary sun-detector tracking. This in effect reduces the heliostat dimension D to facet dimension $\overline{D}$.

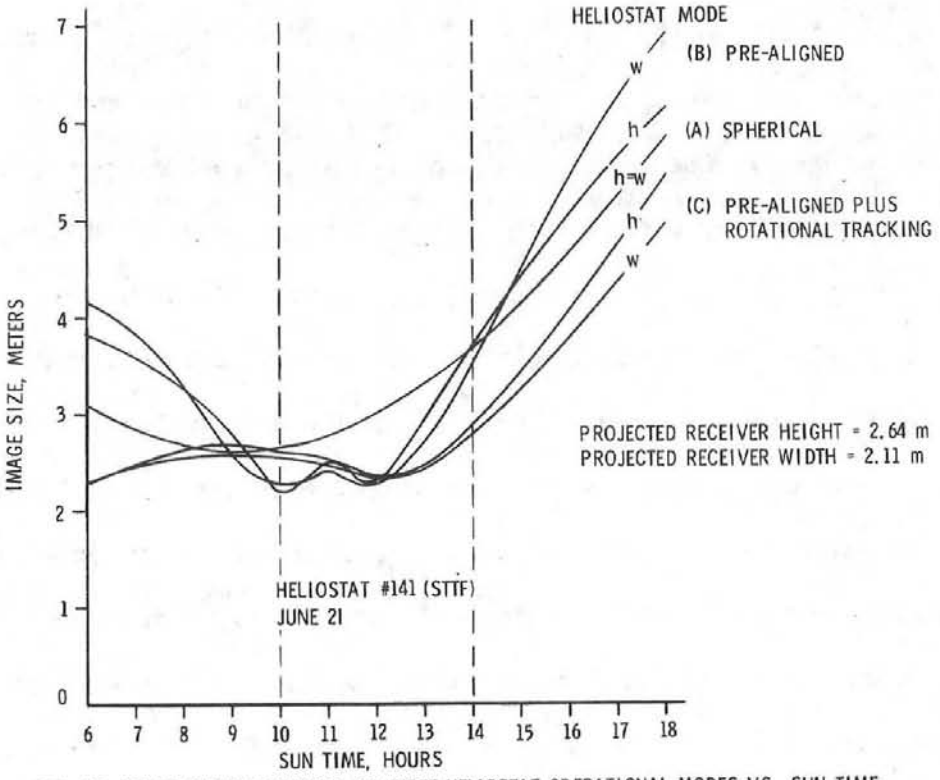

FIG. 17 IMAGE SIZES PRODUCED BY THREE HELIOSTAT OPERATIONAL MODES VS. SUN TIME

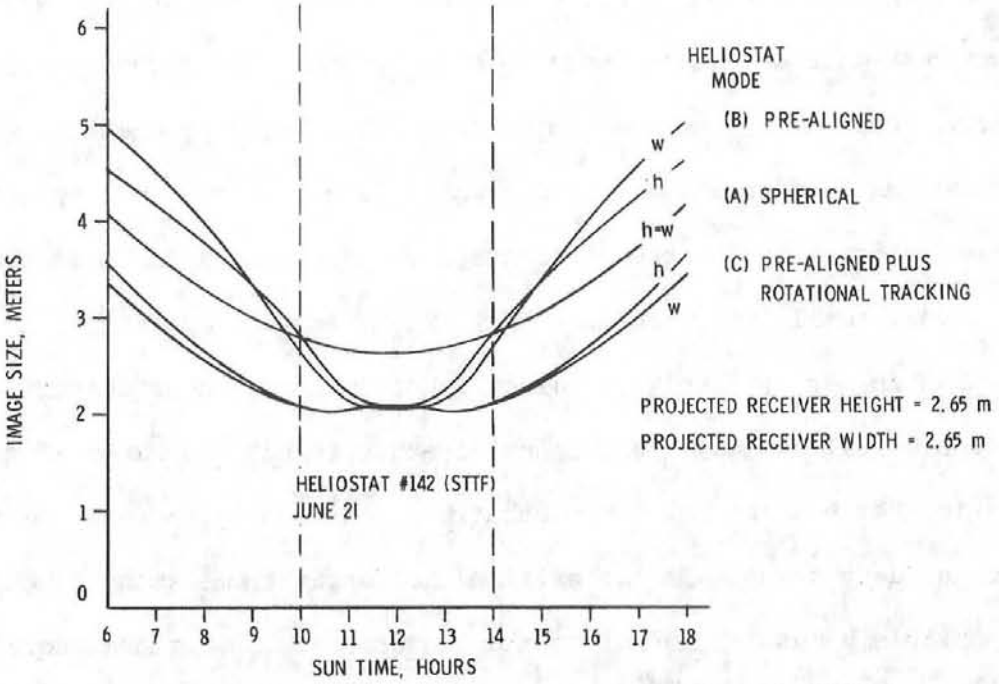

FIG. 18 IMAGE SIZES PRODUCED BY THREE HELIOSTAT OPERATIONAL MODES VS. SUN TIME

2) Alter the angle of pre-alignment, $\bar{\varphi}$. The angle of pre-alignment, $\bar{\varphi}$, may be altered by adjusting the individual facets of a heliostat at given daily time intervals or alternatively by adjusting groups of facets hinged to the heliostat frame at given daily time intervals. Solenoid-actuated wedges or motor-driven jack-nuts programmed by a crude clock might be used to make the adjustments.

3) Reduce the angle of incidence, φ. Angles of incidence, φ, may effectively be reduced by allowing selected portions of pre-aligned heliostat fields to operate over a limited number of hours. The not particularly attractive trade-off here is reduction in overall power level for an increase in operational time.

4) Increase the size of the receiver-aperture, C. Increasing the size of the receiver-aperture is an attractive alternative only when the resultant increase in power received is greater than the power losses which result from a larger receiver-aperture.

While in general large angles of incidence are unavoidable the combination of large angles of incidence coupled with a large incident-angle range, $\Delta\varphi$, presents the most severe challenge. This challenge is maximized for heliostats located on the East-West axis and while those located South of the tower have large angles of incidence, their daily incident angle-range is relatively small, Fig. 11. Note that shadowing of adjacent heliostats which is not considered becomes important at large angles of incidence. Heliostats on the South axis, i.e. South of the tower, have a small daily incident angle-range as shown in Fig. 11. It would appear that an appropriately pre-aligned heliostat would produce minimum image-sizes over a full sun day. Unfortunately this is <u>not</u> <u>true</u> because there is mis-orientation between the rotating operational incident plane and the fixed pre-aligned incident plane. If the existing heliostat frame with attached mirrors were rotatable about the normal to the center facet, (θ continuously adjusted to

equal zero), then improved imaging would be obtained from any heliostat location. An equatorial mount for a heliostat would allow θ to be set equal to zero. Unfortunately, near-perfect imaging for heliostats located South of the tower is automatically de-rated by the $\cos \varphi$ which defines the effective or projected collection area for any heliostat. Performance for these heliostats, neglecting the loss of projected mirror area, would otherwise rate above all others.

Benefits that accrue when the heliostat-frame is rotated or effectively rotated about the normal to the center facet are sufficiently large to seriously consider this option. Improved performance should be carefully balanced against cost of implementation. The conclusion is that if heliostats were to completely surround the tower then the field might be divided into as many as eight segments where the degree of heliostat sophistication and cost is appropriately tailored to the given segment. Increasing orders of heliostat sophistication are as follows:

I. Size the dimension of the heliostat to its location, i.e. slant range.

II. Align heliostat at $\bar{\varphi} = 0$. Spherical mode gives fair average values for image size over full operating time interval, i.e. one sun day.

III. Align heliostat at fixed $\bar{\varphi}$. Pre-aligned mode gives a smaller image size than does condition II for a short operating time interval of two to four hours.

IV. Align heliostat at fixed $\bar{\varphi}$ and rotate the entire heliostat frame about the normal to the center facet. Pre-alignment plus rotational tracking mode gives a smaller average image size than does condition III over a longer operating time interval.

V. Align heliostat at non-fixed $\bar{\varphi}$, i.e. adjust facet alignment at specified daily time intervals with no provision for rotational tracking of the heliostat frame. This in effect makes $\bar{\varphi}$ a variable which is periodically

adjusted to optimally alter the orthogonal radii r_t and r_s for the operational interval between adjustments. Adjustment of $\bar{\varphi}$ automatically includes locating r_t in the operational plane of incidence, i.e. rotational tracking. Carried to the limit we are describing continuous sun tracking by each of the twenty-five facets that comprise a STTF heliostat.

While condition V represents the highest degree of sophistication and results in minimum image sizes, its implementation would no doubt maximize cost.

Using flat surfaced mirrors as opposed to concave spherical reflectors does not negate any of the above general conclusions. The reason is simply that the slope angles at the center of the facets define the heliostat's spherical or toroidal shape while the topography of the individual facet determines the theoretically attainable minimum image size for the heliostat at and near the unique time of alignment.

While the information presented here does not predict the operational insolation levels as does computer code HELIOS[12,13] it does provide insight into the details of optical collection. The computer program HELIOS gives results applicable to heliostat modes (A) and (B) on page 34. With minor modification it should also model heliostat mode (C). One of the major advantages of this evaluation is that the sources of the contributions to image enlargement are identified as well as their magnitude. Thus the recourses available for the reduction of unacceptable image enlargements can also be identified. The analytical predictions provide guide-lines for establishing optical design requirements of heliostats which in turn ultimately determine the economic-feasibility for a Solar Tower Electric Facility. Remember this report considers only optic problems and not heliostat pointing errors, wind loadings, temperature shifts, etc.

Recommendations

Since three dimensional visualizations are somewhat difficult it is proposed that a table-top optical model of an adjustable toroidal mirror with rotational tracking and with system ability to track an artifical sun be constructed to demonstrate the relationships of Eqs. 8 and 9. When using equations 8 and 9 one should consider the fact that the sides of the square heliostat are not generally parallel and perpendicular to the operational incident plane. When this effect is considered (if the heliostat were circular none would exist) the effective dimension, D, of a heliostat might vary from a side to a diagonal dimension. Also it would be useful to program the complete analytical model using a small computer having real time graphic output. Energy enevelopes from individual heliostats and alternatives for design could be quickly visualized and assessed. In the final analysis it is a complex problem to optimize the operation of a solar facility designed to generate electric power and optimization must include total cost-benefit studies, cost-complexity benefits studies, etc.

Additional and different analyses are proposed to describe how one might take advantage of the image at the tangential focus. If this image were made stationary (it rotates with the rotating incident plane) it could then be easily applied to the exterior surface of a cylindrical heat absorber of a type proposed by McDonnell Douglas. As currently envisioned the circular cross-section of the cylindrical receiver is much smaller than its length, ratio of $\simeq 1/17$. This receiver-geometry is ideally suited to astigmatic images.

Appendix A

Depth of Focus for Mirrors Designed for Energy Collection

Consider a concave spherical mirror which forms a minimum size image at its focal length, F. The depth of focus, $d_f = d_{f_1} + |d_{f_2}|$, of the mirror is defined as that distance a target plane may be translated either outside or beyond the focal length, (positive d_{f_1}), or inside the focal length, (negative d_{f_2}), while not exceeding some agreed upon maximum image size. Let the maximum image size equal $(\beta_s + \Delta B)$ F where β_s is the angle subtended by the sun at earth and where ΔB is an incremental angle equal to the allowed angular increase in the size of the image if it were located at the distance F.

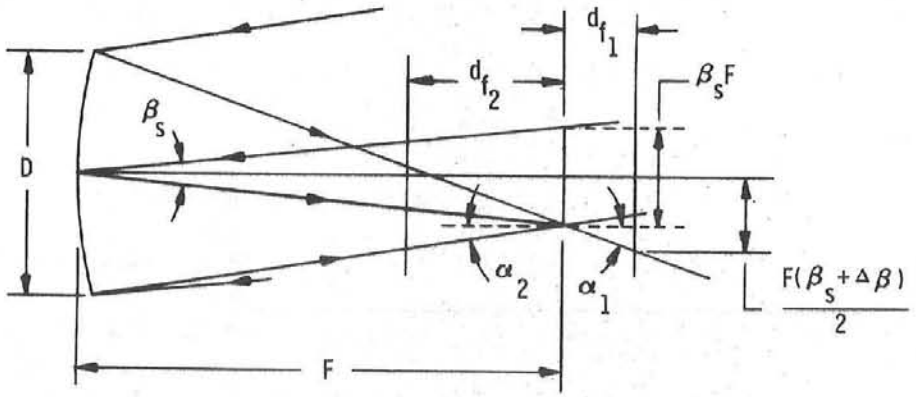

From the geometry we may write

$$\beta_s F + 2\alpha_1 d_{f_1} = F(\beta_s+\Delta B) \qquad \beta_s F + 2\alpha_2 d_{f_2} = F(\beta_s+\Delta B)$$

$$d_{f_1} = F^2(\Delta B)/(\beta_s F+D) \qquad d_{f_2} = F^2(\Delta B)/(\beta_s F-D)$$

where $D > \beta_s F$. If the condition $D > \beta_s F$ is not met then

$$d_{f_1} = \frac{F^2(\Delta B)}{\beta_s F + D} \quad \Big| \quad D < \beta_s F$$

$$d_{f_2} = -F \quad \Big| \quad D < \beta_s F$$

Example

Heliostat #18

$F = 66$ m

$D = 6$ m

$\beta_s = 9.3.10^{-3}$ rad

Let $\Delta\beta = 10^{-3}$ rad

$d_{f_1} = 0.66$ m

$d_{f_2} = -0.81$ m

$d_f = 1.47$ m

Heliostat #141

$F = 220$ m

$D = 6$ m

$\beta_s = 9.3.10^{-3}$ rad

Let $\Delta\beta = 10^{-3}$ rad

$d_{f_1} = 6.0$ m

$d_{f_2} = -12.2$ m

$d_f = 18.3$ m

Appendix B

Heliostat #18 — June 21st — 5 MW Target Projected Area of Receiver-Aperture ≃ 2.45 m^2

Sun Time, hrs.	Angle of Incidence φ, degrees	Linear Dimension l = w, meters	Image Area Collected, %	Total Power Collected, %
6	36.9	1.82	74	53
7	30.0	1.42	100	78
8	23.1	1.09	100	83
9	16.4	0.86	100	86
10	10.1	.71	100	89
11	6.2	.65	100	89
12	8.7	.68	100	90
13	14.7	.81	100	87
14	21.3	1.03	100	84
15	28.2	1.33	100	79
16	35.0	1.70	85	63
17	41.9	2.15	53	36
18	48.6	2.65	35	21

Heliostat #105 — June 21st — 5 MW Target Projected Area of Receiver-Aperture ≃ 6.55 m^2

Sun Time, hrs.	Angle of Incidence φ, degrees	Linear Dimension l = w, meters	Image Area Collected, %	Total Power Collected, %
6	41.1	2.89	78	53
7	35.8	2.55	100	73
8	31.2	2.28	100	77
9	27.8	2.11	100	80
10	26.0	2.02	100	81
11	26.1	2.02	100	81
12	28.2	2.13	100	79
13	31.8	2.31	100	76
14	36.5	2.59	98	71
15	41.9	2.95	75	50
16	47.8	3.38	57	34
17	54.0	3.89	43	23
18	60.4	4.45	33	15

Heliostat #141 June 21st. 5 MW Target Projected Area of Receiver-Aperture ≃ 5.57 m^2

Sun Time, hrs.	Angle of Incidence φ, degrees	Linear Dimension l = w, meters	Image Area Collected, %	Total Power Collected, %
6	34.3	3.09	58	43
7	30.0	2.85	69	54
8	26.9	2.70	76	61
9	25.5	2.63	81	66
10	26.2	2.66	79	64
11	28.7	2.78	72	57
12	32.7	3.00	62	47
13	37.7	3.30	51	36
14	43.2	3.67	41	27
15	49.2	4.13	33	19
16	55.5	4.65	26	13
17	62.0	5.23	20	8
18	68.6	5.86	16	5

Heliostat #142 June 21st. 5 MW Target Projected Area of Receiver-Aperture ≃ 7 m^2

Sun Time, hrs.	Angle of Incidence φ, degrees	Linear Dimension l = w, meters	Image Area Collected, %	Total Power Collected, %
6	51.3	4.07	42	24
7	40.9	3.29	65	44
8	36.5	3.00	78	56
9	33.2	2.81	89	67
10	31.0	2.68	98	76
11	30.4	2.65	100	78
12	31.4	2.70	96	74
13	33.9	2.84	87	65
14	33.9	2.84	87	65
15	37.5	3.06	75	54
16	42.0	3.37	62	41
17	47.1	3.74	50	31
18	52.7	4.19	40	22

Projected area of the receiver aperture is the product of the receiver's projected height and width. The projected receiver height is set equal to the product of the actual receiver height and cosine of σ_h where σ_h is the angle between the receiver heighth and the normal to the ray from the center of the heliostat to the center of the receiver. The projected receiver width is set equal to the product of the actual receiver width and the cosine of σ_w where σ_w is the angle between the receiver width and the normal to the ray from the center of the heliostat to the center of the receiver. Values for σ_h and σ_w are simply obtained from the arc-tangets described by the coordinates of a given heliostat and receiver.

Appendix C

Derivation for Angle τ'

Use a cartesian coordinate system whose orgin is at the intersection of the heliostat's azimuth and elevation axes. Let the plus Z axis be the zenith at that point. The other axes are arbitrary; for example, plus x points East and plus y points North. Let the symbols (a, b, c) be direction cosines. In this system the direction cosines of the sun are

$$(a_s, b_s, c_s)$$

and of the tower

$$(a_t, b_t, c_t) \quad (|c_s, c_t| > 0)$$

The equation of the heliostat-frame plane is

$$a_r x + b_r y + c_r z = 0 \ ,$$

where

$$a_r = (a_s + a_t)/d$$

$$b_r = (b_s + b_t)/d$$

$$c_r = (c_s + c_t)/d$$

$$d = \sqrt{(a_s+a_t)^2 + (b_s+b_t)^2 + (c_s+c_t)^2}$$

The direction cosines of the heliostat's elevation-axis which is the line of intersection of the x-y plane and the heliostat-frame-plane are

$$(a_1, b_1, c_1) = \left(\frac{b_r}{\sqrt{a_r^2+b_r^2}}, \frac{a_r}{\sqrt{a_r^2+b_r^2}}, 0 \right)$$

Define

$$\alpha = c_s b_t - c_t b_s$$

$$\beta = a_s c_t - a_t c_s$$

$$\gamma = a_t b_s - a_s b_t$$

The direction cosines of the normal, ($R_{\theta+90}$ on Fig. 15), to the plane through the sun, tower, and reflector pivot (incident plane) are

$$(a_2, b_2, c_2) = \left(\frac{\alpha}{\sqrt{\alpha^2+\beta^2+\gamma^2}}, \frac{\beta}{\sqrt{\alpha^2+\beta^2+\gamma^2}}, \frac{\gamma}{\sqrt{\alpha^2+\beta^2+\gamma^2}} \right)$$

Then

$$\tau' = \cos^{-1} [a_1 a_2 + b_1 b_2] \Big|_{c_1 = 0}$$

References

1. H. E. Paine, British Patent in 1893, Nos. 22,837; 22,939; 22,338

2. T. D. Brumleve, "A High-temperature Solar Energy System", Sandia Laboratories Livermore, SAND74-8008, August 1974.

3. L. M. Murphy, A. C. Skinrood, "Development of the Solar Power Central Receiver Concept", Sandia Laboratories Livermore, SAND76-8677, September 1976.

4. V. A. Baum, R. R. Aparisi, and B. A. Garf, "High Power Solar Installations", Solar Energy 1, 6(1957).

5. Lorin L. Vant-Hull, "Development Of Solar Tower Program In The United States", SPIE Vol. 85, Optics In Solar Energy Utilization, 1976.

6. R. H. McFee, "Power Collection Reduction By Mirror Surface Nonflatness And Tracking Error For A Central Receiver Solar Power System", Applied Optics, Vol. 14, No. 7, July 1975.

7. Henry Coddington, "An Elementary Treatise on Optics", Printed by T. Smith for F. Deighton & Sons, 2nd Edition, 1825.

8. R. S. Longhurst, "Geometrical And Physical Optics", Longmans Green and Co., Great Britain, 1957, pgs. 334-335.

9. F. Biggs and C. N. Vittitoe, "Parameter Study For Central Receiver Power Stations", Sandia Laboratories Albuquerque, SAND77-0677C. April 1977.

10. E. A. Aronson, Div. 2642, Private Communication. See Appendix C.

11. L. C. Martin, W. T. Welford, "Technical Optics", Vol. I, Pitman Publishing Corp., New York, N. Y. 1966 pgs. 330-331.

12. C. N. Vittitoe, Frank Biggs, R. E. Lighthill, "HELIOS: A Computer Program For Modeling The Solar Thermal Test Facility", Sandia Laboratories Albuquerque, SAND76-0346.

13. F. Biggs and C. N. Vittitoe, "Mathematical Modeling of Solar Concentrators", Joint Conference, American Section, International Solar Energy Society and Solar Energy Society of Canada, Inc., Vol. 2 Solar Collectors, August 1976.

Acknowledgements

The authors wish to thank Garth Gobeli for many helpful discussions which challenged and encouraged the development of this report. We also wish to thank George Bott for obtaining all experimental results and, George Bott and Henry Tendall for preparation of the report figures. We appreciate the help of E. A. Aronson, Org. 2642 for his analysis given in Appendix C and special thanks are due K. R. Hessel, Org. 2542 and Frank Biggs, Org. 5231 for their instructive reviews.

Distribution
(Unlimited Release)

2000 E. D. Reed
2500 J. C. King
2532 G. R. Bachand
2541 G. W. Gobeli
2541 E. A. Igel (20)
2541 R. L. Hughes
2541 K. W. Chu
2541 D. M. Fenstermacher
2541 L. K. Galbraith
2541 P. J. Hargis, Jr.
2541 J. P. Hohimer
2541 M. M. Robertson
2541 K. T. Stalker
2541 A. E. McCarthy
2541 G. F. Bott
2541 M. F. Johnson
2541 S. A. Palmer
2541 M. E. Wilkins
2542 K. R. Hessel
2542 M. J. Landry
2642 E. A. Aronson
3442 L. L. Young
3721 F. G. Higgins
5214 M. A. Palmer
5217 R. A. Hill
5231 F. Biggs
5231 C. N. Vittitoe
5700 J. H. Scott
5710 G. E. Brandvold
5711 J. F. Banas
5712 L. A. Leonard
5713 J. V. Ott (10)
5713 R. D. Aden
5713 G. A. Anderson
5713 J. E. Clark
5713 D. B. Davis
5713 R. M. Edgar
5713 J. T. George
5713 J. T. Holmer
5713 D. J. Kuehl
5713 L. K. Matthews
5713 J. E. Meyers
5713 L. O. Seamons
5713 J. M. Stomp
5714 R. P. Stromberg
5715 R. H. Braasch
5715 R. C. Reuter
5719 D. G. Schueler
5742 S. G. Varnado
8130 R. C. Wayne
8132 T. D. Brumleve
8132 A. C. Skinrood
8132 Clifford Yokomizo
8180 C. S. Selvage
8322 J. D. Hankins
9352 J. C. Bushnell
9410 R. L. Brin
9412 R. K. Petersen
9412 D. L. Fastle
9412 J. S. Llamas
9412 G. S. Phipps
9412 C. E. Robertson
9412 I. W. Janney
9420 T. L. Pace
8266 E. A. Aas (2)
3131 C. A. Pepmueller, Actg. (5)
3151 W. L. Garner (3)
For ERDA/TIC
3171-1 R. P. Campbell (25)